Selective cell death of oncogenic Akt-transduced brain cancer cells by etoposide through reactive oxygen species–mediated damage

Se-Yeong Oh,[1] Young-Woo Sohn,[1] Jong-Whi Park,[1] Hyo-Jung Park,[1] Hye-Min Jeon,[1] Tae-Kyung Kim,[1] Joong-Seob Lee,[1] Ji-Eun Jung,[1] Xun Jin,[1] Yong Gu Chung,[2] Young-Ki Choi,[3] Seungkwon You,[1] Jang-Bo Lee,[2] and Hyunggee Kim[1]

[1]The Laboratories of Cell Growth and Function Regulation, Division of Biotechnology, College of Life Sciences and Biotechnology and [2]Department of Neurosurgery, School of Medicine, Korea University, Seoul, Republic of Korea and [3]Department of Microbiology, Medical Research Institute, College of Medicine, Chungbuk National University, Cheongju, Republic of Korea

Abstract

We have established several glioma-relevant oncogene-engineered cancer cells to reevaluate the oncogene-selective cytotoxicity of previously well-characterized anticancer drugs, such as etoposide, doxorubicin, staurosporine, and carmustine. Among several glioma-relevant oncogenes (activated epidermal growth factor receptor, Ras, and Akt, as well as Bcl-2 and p53DD used in the present study), the activated epidermal growth factor receptor, Ras, and Akt exerted oncogenic transformation of Ink4a/Arf$^{-/-}$ murine astrocyte cells. We identified that etoposide, a topoisomerase II inhibitor, caused selective killing of myristylated Akt (Akt-myr)–transduced Ink4a/Arf$^{-/-}$ astrocytes and U87MG cells in a dose- and time-dependent manner. Etoposide-selective cytotoxicity in the Akt-myr–transduced cells was shown to be caused by nonapoptotic cell death and occurred in a p53-independent manner. Etoposide caused severe reactive oxygen species (ROS) accumulation preferentially in the Akt-myr–transduced cells, and elevated ROS rendered these cells highly sensitive to cell death. The etoposide-selective cell death of Akt-myr–transduced cells was attenuated by pepstatin A, a lysosomal protease inhibitor. In the present study, we show that etoposide might possess a novel therapeutic activity for oncogenic Akt-transduced cancer cells to kill preferentially through ROS-mediated damage. [Mol Cancer Ther 2007;6(8):2178–87]

Received 2/19/07; revised 5/21/07; accepted 6/29/07.

Grant support: Korea Food and Drug Administration grant 07132KFDA689 in 2007 and a Biogreen 21 grant (H. Kim).

The costs of publication of this article were defrayed in part by the payment of page charges. This article must therefore be hereby marked *advertisement* in accordance with 18 U.S.C. Section 1734 solely to indicate this fact.

Requests for reprints: Hyunggee Kim, Division of Biotechnology, College of Life Sciences and Biotechnology, Korea University, 5-ka, Anam-dong, Seongbuk-gu, Seoul 136-713, Republic of Korea. Phone: 82-2-3290-3059. E-mail: hg-kim@korea.ac.kr; or Jang-Bo Lee, Department of Neurosurgery, School of Medicine, Korea University, Seoul, Republic of Korea. E-mail: jangbo@korea.ac.kr

doi:10.1158/1535-7163.MCT-07-0111

Introduction

Among numerous human tumors, malignant astrocytoma, one of the most common brain tumors, has proven to be extremely resistant to various anticancer therapies, such as chemotherapy and radiation. A variety of extensive molecular and genetic studies have identified the frequently deregulated genes and their related signaling pathways. The most commonly activated genes (including signaling pathways) are *epidermal growth factor receptor* (*EGFR*), *RAS, phosphatidylinositol 3-kinase/Akt, cyclin-dependent kinase 4*, and *cyclin D1*, whereas the frequently inactivated genes include *p53, INK4a/ARF*, and *PTEN* tumor suppressors (1). In addition, the biological relevance of these genetic alterations in the development of human brain tumors has been shown by various *in vitro* and *in vivo* mouse model studies (2).

The identification of specific oncogenes relevant to tumorigenesis and understanding the molecular and cell signaling differences between normal and cancer cells are essential research areas in the development of particular oncogene-selective anticancer drugs. Two promising examples in the development of oncogene-targeted anticancer therapeutics are Gleevec (imatinib mesylate) and Herceptin (trastuzumab), which target the oncogenic tyrosine kinase BCR-ABL protein (one of the major culprits in the development of human chronic myeloid leukemia) and HER2/NEU oncoprotein responsible for human malignant breast cancers, respectively (3, 4).

Although an ideal anticancer drug should be cytotoxic to cancer cells with limited side effects on normal cells, there are restricted numbers of such anticancer drugs available for clinical use. Therefore, the new approach for discovery of such compounds is the reevaluation of previously known anticancer drugs and/or the identification of novel anticancer drugs using cancer cell lines that are genetically modified by the introduction of oncogenic molecules of interest (5).

In this regard, using astrocyte cells derived from Ink4a/Arf tumor suppressor knockout mouse and human U87MG glioma cells, we first established several genetically modified cancer cell lines by transduction of different glioma-related oncogenes (activated EGFR, Ras, and Akt, as well as Bcl-2 and p53DD) and then reevaluated the particular oncogene-dependent cytotoxicities of previously known anticancer compounds, such as etoposide, doxorubicin, staurosporine, and carmustine.

Materials and Methods

Astrocyte Preparation and Cell Culture

Primary cortical astrocytes were isolated from 5-day-old pups and prepared according to published methods (6). Cells were maintained in DMEM containing 10% fetal bovine serum (Hyclone), 1% penicillin and streptomycin (Life Technologies), and 1% L-glutamine (Life Technologies). To determine cell growth rates, cells were plated at a density of 2.5×10^4 to 5.0×10^4 cells per six-well plate. Five days after cell plating, cell numbers were counted using a hematocytometer.

Plasmids and Retrovirus Production

PT67 cells were transfected with various oncogenes (cloned into pBabe-Puro) using LipofectAMINE 2000 (Invitrogen) according to the protocol of the manufacturer. The Ink4a/Arf$^{-/-}$ astrocytes and U87MG cells that had been plated 24 h earlier at 1×10^6 cells/10-cm dish were infected with prefiltered (0.45 μm) retroviral supernatant (produced from PT67 cells) containing 6 μg/mL of polybrene (Sigma). Infected cells were selected with puromycin or G418 for 7 to 12 days.

In vivo Transplantation Studies

Ink4a/Arf$^{-/-}$ astrocyte cells (1×10^6) were injected s.c. ($n = 6$ for each transfectant). Cells were washed and resuspended in PBS (1×10^6 cells in 100 μL), placed on ice, and injected into nude mice (BALB/c$^{-/-}$).

Soft Agar Assay and Clonogenic Assay

To examine anchorage-independent growth, Ink4a/Arf$^{-/-}$ astrocytes (1×10^4) infected with pBabe-Puro, pBabe-Akt-myr, pBabe-Bcl-2, pBabe-EGFR*, pBabe-H-ras^{V12}, and pBabe-p53DD, as well as HeLa cells (positive control), were cultured into six-well soft agar dishes (1.6% and 0.7% bottom and top agar, respectively) for 3 weeks.

To determine long-term survival in the presence of the etoposide, U87MG cells transduced with pBabe-Puro and pBabe-Akt-myr were cultured into six-well soft agar dish containing different concentration of etoposide (0, 10, 50, 100, 250, and 500 μmol/L) in the top agar. Then, DMEM (1 mL) supplemented with 10% fetal bovine serum and the indicated concentration of etoposide was added on top of each well everyday for 14 days. Foci numbers of U87MG cells were counted at 14 days.

Western Blot Analysis

Whole-cell extracts were prepared using radioimmunoprecipitation assay lysis buffer containing 1 mmol/L β-glycerophosphate, 2.5 mmol/L sodium pyrophosphate, 1 mmol/L NaF, 1 mmol/L Na_3VO_4, and protease inhibitor (Roche). Protein in the extracts (30–100 μg) was separated by a 4% to 12% gradient or 10% SDS-PAGE NuPAGE gel (Invitrogen) and was then transferred to a polyvinylidene difluoride membrane (Millipore). The membranes were blocked with 5% nonfat milk and incubated with anti-Akt (Cell Signaling), Bcl-2 (c-2, Santa Cruz Biotechnology), anti-p53 (Ab-1, Oncogene for p53DD protein), anti-p21^{WAF1} (C-19, Santa Cruz Biotechnology), anti-Bax (N-20, Santa Cruz Biotechnology), anti-EGFR (Santa Cruz Biochemistry), anti–c-H-ras (Oncogene), anti–caspase-3 (Santa Cruz Biotechnology), and anti–α-tubulin (Sigma) antibodies. Membranes were then incubated with horseradish peroxidase–conjugated anti-secondary IgG (Pierce) antibody and visualized with SuperSignal West Pico Chemiluminescent Substrate (Pierce).

Quantification of Sub-G_1 DNA Content

The cell population possessing <2N was determined by flow cytometry using a FACSCalibur equipped with CellQuestPro software. Cells were fixed with 70% cold ethanol and resuspended with 200 μL of 100 μg/mL propidium iodide in PBS.

Determination of Cellular Reactive Oxygen Species

Cellular reactive oxygen species (ROS) contents were measured as described (7) with a minor modification. The control or drug-treated Ink4a/Arf$^{-/-}$ astrocyte cells were incubated with 5 μmol/L 2′,7′-dichlorofluorescein diacetate (Calbiochem) for 30 min, followed by flow cytometry using a FACSCalibur equipped with CellQuestPro software. For U87MG glioblastoma cells, 10 μmol/L 2′,7′-dichlorofluorescein diacetate was used in 30 min labeling to obtain sufficient fluorescence signals.

Assays for Cytotoxicity

The trypan blue exclusion method was used to assess the viability and death rates of cells grown in the absence or presence of different concentrations of antitumor compounds [30 mg/mL carmustine [1,3-bis(2-chloroethyl)-1-nitrosourea], Sigma; 50 nmol/L staurosporine, Calbiochem; 60 μmol/L etoposide, Sigma; and 100 μmol/L doxorubicin, Sigma].

Cell death was determined by flow cytometry after cells were double stained with Annexin V-FITC (BD PharMingen) at a dilution of 1:100 and with 50 μg/mL propidium iodide (Sigma). The percentage of cells was determined by flow cytometry using a FACSCalibur equipped with CellQuestPro software. The cells were treated with pepstatin A (2 mmol/L in DMSO; Calbiochem), *N*-acetyl-L-cysteine (10 mmol/L in H_2O; Calbiochem), and Paraquat (2 mmol/L in H_2O; Sigma).

Reverse Transcription-PCR

Total RNA was isolated from cells using Trizol (Life Technologies) according to the instructions of the manufacturer. For semiquantitative reverse transcription-PCR, 3 μg DNase I–treated RNA was converted to cDNA with SuperScript II reverse transcriptase (Invitrogen) according to the instructions of the manufacturer. A portion (1 μL) of the reverse transcription reaction was used to amplify p21^{WAF1} and glyceraldehyde-3-phosphate dehydrogenase cDNA fragments using the following primer sets: human p21^{WAF1}: 5′-ttagcagcggaacaaggagt-3′ (forward) and 5′-attcagcattgtgggaggag-3′ (reverse) and human glyceraldehyde-3-phosphate dehydrogenase 5′-ctacactgagcaccaggtggtctc-3′ (forward) and 5′-gatggatacatgacaaggtgcggc-3′ (reverse). All reverse transcription-PCR amplifications were verified to be in the linear range. Information about PCR variables used in the reverse transcription-PCR will be provided on request.

Statistical Analysis

All experiments were replicated three times at least. Data were analyzed statistically using Duncan's test in SAS

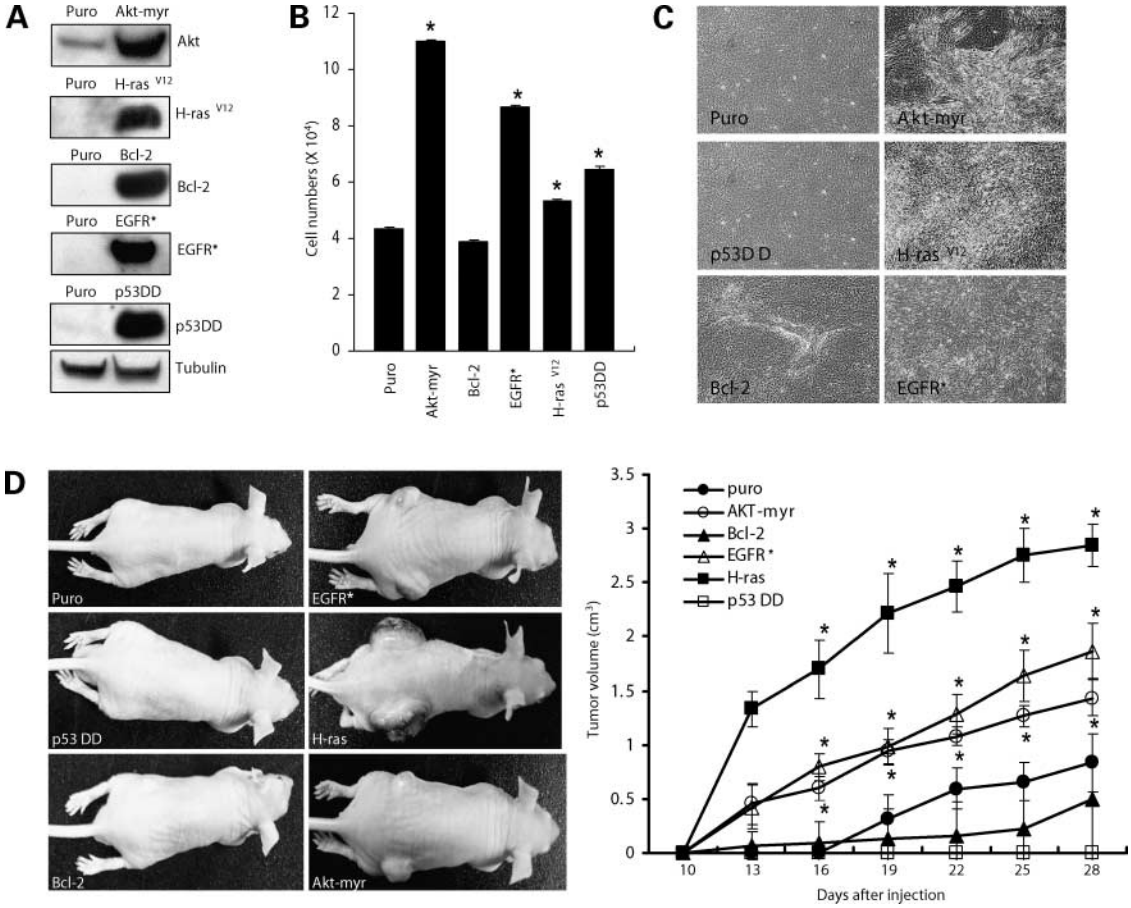

Figure 1. Oncogenic transformation of Ink4a/Arf$^{-/-}$ murine astrocyte cells by a variety of oncogenes. **A,** overexpression of Akt-myr, H-ras^{V12}, Bcl-2, EGFR*, and p53DD in Ink4a/Arf$^{-/-}$ astrocyte cells was determined by Western blot analysis. **B,** *in vitro* growth rates of Ink4a/Arf$^{-/-}$ astrocyte cells transduced with control vector (Puro), Akt-myr, Bcl-2, EGFR*, H-ras^{V12}, and p53DD were determined by the counting of cells 5 d after plating. *Columns,* mean (n = 3); *bars,* SE. *, $P < 0.05$, significant difference. **C,** representative photos showing confluent cell morphology of Ink4a/Arf$^{-/-}$ astrocyte cells that were transduced with control vector, Akt-myr, Bcl-2, EGFR*, H-ras^{V12}, and p53DD. Only one region of Bcl-2–transduced Ink4a/Arf$^{-/-}$ astrocyte cells grown in the 10-cm culture dish was shown to be piled up. **D,** representative photos (*left*) showing nude mice injected s.c. with Ink4a/Arf$^{-/-}$ astrocyte cells transduced with control vector, Akt-myr, Bcl-2, EGFR*, H-ras^{V12}, and p53DD. Tumor growth rate (*right*) in the nude mice injected s.c. with Ink4a/Arf$^{-/-}$ astrocyte cells transduced with control vector, Akt-myr, Bcl-2, EGFR*, H-ras^{V12}, and p53DD. *Points,* mean (n = 6); *bars,* SE. *, $P < 0.05$, shown in the tumor volumes of Akt-myr–, EGFR*-, and H-ras^{V12}-transduced Ink4a/Arf$^{-/-}$ astrocyte cells compared with control (Puro) cells indicates a significant difference.

software package (version 9.1). The level of statistical significance was based on the P values ($P < 0.05$).

Results

Oncogenic Transformation of Ink4a/Arf$^{-/-}$ Murine Astrocyte Cells by a Variety of Oncogenes

To establish genetically engineered mouse astrocytoma cell models, we transduced various oncogenes, such as a myristylated Akt (Akt-myr), H-ras^{V12}, Bcl-2, a constitutively active EGFR-deleted form (EGFR*), and dominant-negative p53 (p53DD), all of which are associated with tumorigenesis in a variety of human and mouse brain tumors (1), into Ink4a/Arf$^{-/-}$ murine astrocyte cells. We first determined whether Ink4a/Arf$^{-/-}$ astrocyte cells transduced with different oncogenes possess oncogenically transformed phenotypes *in vitro* and *in vivo*. As shown in Fig. 1A, overexpression of Akt-myr, H-ras^{V12}, Bcl-2, EGFR*, and p53DD in Ink4a/Arf$^{-/-}$ astrocyte cells was determined by Western blot analysis. Akt-myr–, EGFR*-, H-ras^{V12}–, and p53DD-transduced Ink4a/Arf$^{-/-}$ astrocyte cells, but not Bcl-2–transduced cells, were found to grow faster *in vitro* than pBabe-Puro–transduced Ink4a/Arf$^{-/-}$ astrocyte cells (Fig. 1B). Unlike Puro-, p53DD-, and Bcl-2–transduced Ink4a/Arf$^{-/-}$ astrocyte cells, Akt-myr–, H-ras^{V12}–, and EGFR*-transduced Ink4a/Arf$^{-/-}$ astrocyte cells showed the loss of density-dependent inhibition of growth, with the piling-up of foci displaying a unique morphology (Fig. 1C) and anchorage-independent growth in the soft agar culture conditions (Supplementary Fig. S1A).[4]

[4] Supplementary material for this article is available at Molecular Cancer Therapeutics Online (http://mct.aacrjournals.org/).

Furthermore, Akt-myr-Ink4a/Arf$^{-/-}$, H-ras^{V12}-Ink4a/Arf$^{-/-}$, and EGFR*-Ink4a/Arf$^{-/-}$ astrocyte cells injected s.c. into nude mice were shown to be tumorigenic *in vivo* (Fig. 1D, *left*). Tumor masses of Akt-myr-Ink4a/Arf$^{-/-}$, H-ras^{V12}-Ink4a/Arf$^{-/-}$, and EGFR*-Ink4a/Arf$^{-/-}$ astrocyte cells were dramatically increased within 2 weeks compared with those of Puro-, Bcl-2–, and p53DD-transduced of Ink4a/Arf$^{-/-}$ astrocyte cells (Fig. 1D, *right*). These results indicate that activated Akt, Ras, and EGFR, which are commonly activated in different grades of human astrocytomas (1), are strong inducers for oncogenic transformation of Ink4a/Arf$^{-/-}$ murine astrocyte cells.

Cell Death Response of the Oncogene-Transduced Ink4a/Arf$^{-/-}$ Astrocyte Cells to Various Anticancer Drugs

To identify particular oncogene-targeted anticancer drugs, we first treated different oncogene-transduced Ink4a/Arf$^{-/-}$ astrocyte cells with staurosporine (a pan-kinase inhibitor) and doxorubicin, carmustine, and etoposide (DNA-damaging agents). Both control and oncogene-transduced Ink4a/Arf$^{-/-}$ astrocyte cells showed a similar cell death response to staurosporine (Fig. 2A). Akt-myr–, Bcl-2–, H-ras^{V12}–, and p53DD-transduced Ink4a/Arf$^{-/-}$ astrocyte cells showed significant resistance to cell death, whereas EGFR*-transduced cells displayed relative sensitivity to cell death by doxorubicin treatment compared with control cells (Fig. 2B). Compared with control cells, all oncogene-transduced Ink4a/Arf$^{-/-}$ astrocyte cells tested here were shown to be resistant to cell death by carmustine treatment (Fig. 2C). Interestingly, both Akt-myr– and H-ras^{V12}–transduced Ink4a/Arf$^{-/-}$ astrocyte cells, but not other oncogene-transduced cells, showed significant sensitivity to cell death by etoposide treatment compared with control cells (Fig. 2D).

Because doxorubicin and etoposide are well-known inducers of DNA damage by inhibiting topoisomerase II, we assumed that the etoposide-sensitive, not doxorubicin-specific, cell death of Akt-myr– and H-ras^{V12}–transduced Ink4a/Arf$^{-/-}$ astrocyte cells may occur independently of the topoisomerase II inhibition-induced DNA damage response. As shown in Fig. 2D, because the Akt-myr–transduced Ink4a/Arf$^{-/-}$ astrocyte cells showed slightly higher sensitivity to cell death by etoposide treatment compared with H-ras^{V12}–transduced cells, we focused further studies on using the Akt-myr–transduced Ink4a/Arf$^{-/-}$ astrocyte cells to determine the possible mechanism underlying etoposide-sensitive cell death.

Dose- and Time-Dependent Cell Death Response of Oncogene-Transduced U87MG and Ink4a/Arf$^{-/-}$ Astrocyte Cells to Etoposide

To further examine the cell death sensitivity of Akt-myr–transduced Ink4a/Arf$^{-/-}$ astrocyte cells to etoposide treatment, we assessed the dose-dependent cell death response on treatment of pBabe-Puro–, Akt-myr–, EGFR*-, and Bcl-2–transduced Ink4a/Arf$^{-/-}$ astrocyte cells with different concentrations of etoposide (0, 1, 5, 10, 100, and 500 μmol/L) for 48 h. As shown in Fig. 3A, Akt-myr–transduced Ink4a/Arf$^{-/-}$ astrocyte cells displayed more sensitivity in cell death at each of the different concentrations (except 500 μmol/L, in which all cells tested died) of etoposide compared with control cells. Interestingly, Bcl-2–transduced Ink4a/Arf$^{-/-}$ astrocyte cells showed more sensitivity in cell death to lower concentrations of etoposide (1, 5, and 10 μmol/L), whereas

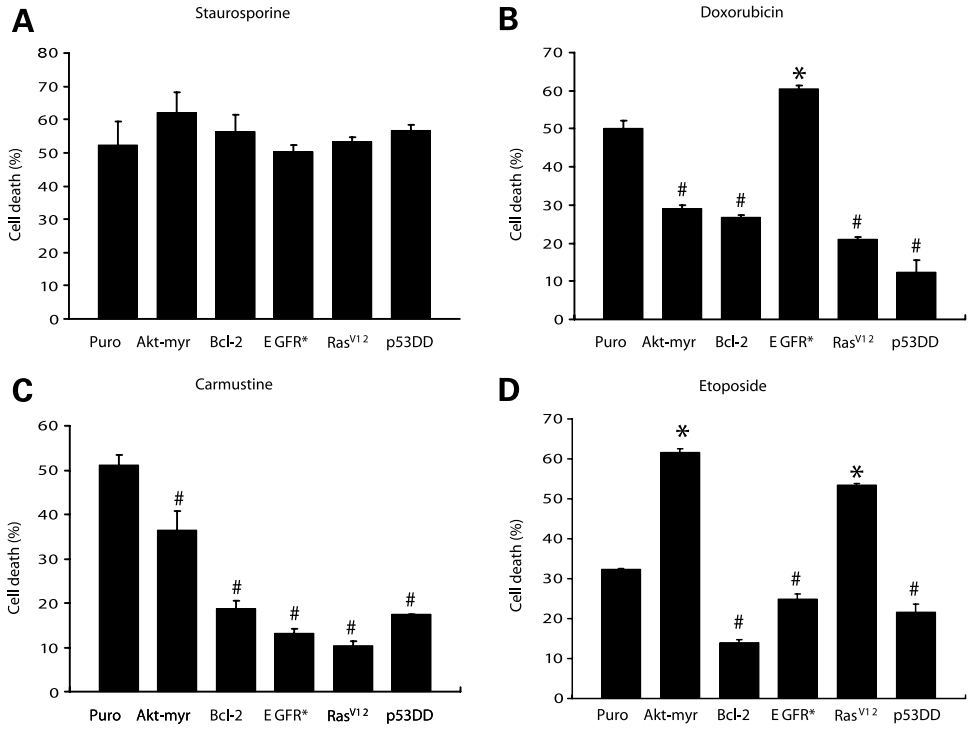

Figure 2. Cell death response of the oncogene-transduced Ink4a/Arf$^{-/-}$astrocyte cells to various anticancer drugs. **A,** cell death rates of Ink4a/Arf$^{-/-}$ astrocyte cells transduced with control vector, Akt-myr, Bcl-2, EGFR*, H-ras^{V12}, and p53DD by staurosporine treatment. *Columns,* mean (n = 3); *bars,* SE. **B,** cell death rates of Ink4a/Arf$^{-/-}$ astrocyte cells transduced with control vector, Akt-myr, Bcl-2, EGFR*, H-ras^{V12}, and p53DD by doxorubicin treatment. *Columns,* mean (n = 3); *bars,* SE. *, $P < 0.05$, significant sensitivity to cell death; #, $P < 0.05$, significant resistance to cell death. **C,** cell death rates of Ink4a/Arf$^{-/-}$ astrocyte cells transduced with control vector, Akt-myr, Bcl-2, EGFR*, H-ras^{V12}, and p53DD by carmustine treatment. *Columns,* mean (n = 3); *bars,* SE. #, $P < 0.05$, significant resistance to cell death. **D,** cell death rates of Ink4a/Arf$^{-/-}$ astrocyte cells transduced with control vector, Akt-myr, Bcl-2, EGFR*, H-ras^{V12}, and p53DD by etoposide treatment. *Columns,* mean (n = 3); *bars,* SE. *, $P < 0.05$, significant sensitivity to cell death; #, $P < 0.05$, significant resistance to cell death.

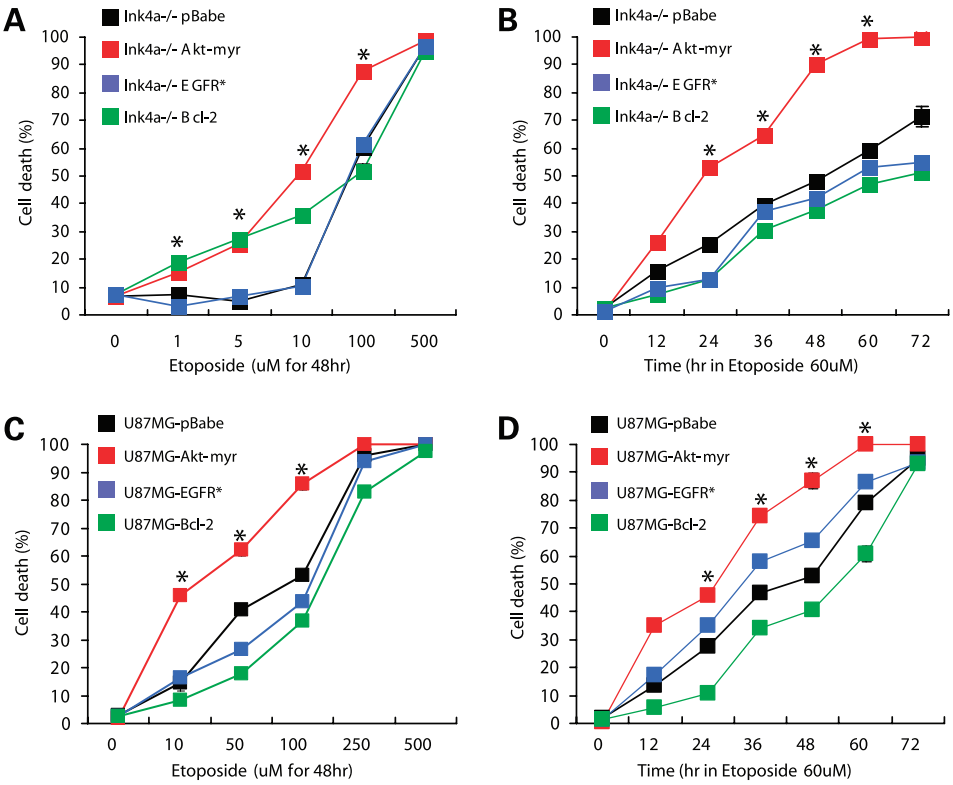

Figure 3. Dose- and time-dependent cell death response of oncogene-transduced U87MG and Ink4a/Arf$^{-/-}$ astrocyte cells to etoposide. **A,** dose-dependent cell death responses of Ink4a/Arf$^{-/-}$ astrocyte cells transduced with control vector, Akt-myr, EGFR*, and Bcl-2 to etoposide (0, 1, 5, 10, 100, and 500 μmol/L) for 48 h. *Points,* mean (n = 3); *bars,* SE. *, $P < 0.01$, significant difference between Akt-myr− and Puro-transduced Ink4a/Arf$^{-/-}$ astrocyte cells. **B,** time-dependent cell death responses of Ink4a/Arf$^{-/-}$ astrocyte cells transduced with control vector, Akt-myr, EGFR*, and Bcl-2 to etoposide (60 μmol/L) for 0, 12, 24, 36, 48, 60, and 72 h. *Points,* mean (n = 3); *bars,* SE. *, $P < 0.01$, significant difference between Akt-myr− and Puro-transduced Ink4a/Arf$^{-/-}$ astrocyte cells. **C,** dose-dependent cell death responses of U87MG cells transduced with control vector, Akt-myr, EGFR*, and Bcl-2 to etoposide (0, 10, 50, 100, 250, and 500 μmol/L) for 48 h. *Points,* mean (n = 3); *bars,* SE. *, $P < 0.01$, significant difference between Akt-myr− and Puro-transduced U87MG cells. **D,** time-dependent cell death responses of U87MG cells transduced with control vector, Akt-myr, EGFR*, and Bcl-2 to etoposide (60 μmol/L) for 0, 12, 24, 36, 48, 60, and 72 h. *Points,* mean (n = 3); *bars,* SE. *, $P < 0.01$, significant difference between Akt-myr− and Puro-transduced U87MG cells.

a similar cell death response was observed at the higher concentrations of etoposide (100 and 500 μmol/L) compared with control cells. We next analyzed the time-dependent cell death response by treatment of these Ink4a/Arf$^{-/-}$ astrocyte cells with etoposide (60 μmol/L) for different lengths of time (0, 12, 24, 36, 48, 60, and 72 h). Akt-myr–transduced Ink4a/Arf$^{-/-}$ astrocyte cells showed significantly more sensitivity in cell death in the presence of etoposide at each of the durations of treatment compared with control cells (Fig. 3B).

We next compared etoposide-dependent cell death sensitivity with the human U87MG glioma cell line transduced with pBabe-Puro control vector, Akt-myr, EGFR*, and Bcl-2. We determined a dose-dependent cell death response on treatment of pBabe-Puro−, Akt-myr−, EGFR*-, and Bcl-2–transduced U87MG cells with different concentrations of etoposide (0, 10, 50, 100, 250, and 500 μmol/L) for 48 h. Similar to Akt-myr–transduced Ink4a/Arf$^{-/-}$ astrocyte cells, Akt-myr–transduced U87MG cells showed more sensitivity in cell death at each of the different concentrations (except 250 and 500 μmol/L, in which most of the cells tested died) of etoposide compared with control cells (Fig. 3C). We then examined the time-dependent cell death response by treatment of these U87MG cells with etoposide (60 μmol/L) for different lengths of time (0, 12, 24, 36, 48, 60, and 72 h). Akt-myr–transduced U87MG cells showed significantly more sensitivity in cell death in the presence of etoposide at each of the durations of treatment (except 72 h at which all cells tested died) compared with control cells (Fig. 3D).

Furthermore, we conducted a clonogenic assay using soft agar culture condition to explore whether overexpression of Akt-myr in the Ink4a/Arf$^{-/-}$ astrocytes and U87MG cells also has an effect on long-term survival in the presence of different concentration of etoposide. As shown in Supplementary Fig. S1B,[4] foci numbers of the Akt-myr–transduced U87MG cells were markedly reduced in the presence of 100 μmol/L etoposide compared with their control counterpart.

We also compared the sensitized cell death response of Akt-myr–transduced Ink4a/Arf$^{-/-}$ murine astrocytes and human U87MG cells following treatment with etoposide with that of these cells treated with doxorubicin. Akt-myr–transduced Ink4a/Arf$^{-/-}$ astrocyte cells displayed significantly more resistance in cell death by doxorubicin treatment in a dose- and time-dependent manner compared with treatment with etoposide (Supplementary Fig. S2).[4]

Nonapoptotic Cell Death of Oncogenic Akt-Transduced U87MG and Ink4a/Arf$^{-/-}$ Astrocyte Cells by Etoposide

To evaluate whether etoposide-dependent cell death is caused by apoptosis, apoptotic cell death of U87MG-pBabe and U87MG-Akt-myr cells treated with etoposide was measured by fluorescence-activated cell sorting (FACS)–based quantification of the sub-G_1 cell population. Interestingly, there was no significant change in sub-G_1 population between U87MG-pBabe and U87MG-Akt-myr cells treated with etoposide (60 μmol/L) for 24 h (Fig. 4A). Consistent with the findings for U87MG cells, Ink4a/Arf$^{-/-}$ astrocyte-Puro and Ink4a/Arf$^{-/-}$ astrocyte-Akt-myr cells showed no significant difference in sub-G_1 population after treatment with etoposide (data not shown). We next conducted Western blot analysis to determine the levels of activated caspase-3 (a hallmark of apoptosis) in the Ink4a/Arf$^{-/-}$ astrocytes and U87MG cells. As shown in Fig. 4B, activated caspase-3 was barely detectable in the Ink4a/Arf$^{-/-}$ astrocyte-Puro and Ink4a/Arf$^{-/-}$ astrocyte-Akt-myr cells (as well as U87MG-Puro and U87MG-Akt-myr cells; data not shown) grown in the absence or presence of etoposide (60 μmol/L) for 24 h, whereas activated caspase-3 was markedly increased in BJ fibroblast cells (as positive control) treated with either etoposide or staurosporine. We then measured apoptotic and nonapoptotic cell death of the Ink4a/Arf$^{-/-}$ astrocytes (Puro and Akt-myr) and U87MG (Puro and Akt-myr) cells treated without or with etoposide (60 μmol/L for 24 h) by propidium iodide/Annexin V-FITC staining and FACS-based quantification. No significant difference was observed in the apoptotic cell population (right upper and right lower windows that possess propidium iodide–positive + Annexin V–positive cell population and propidium iodide–negative + Annexin V–positive cell population, respectively) in the Ink4a/Arf$^{-/-}$ astrocyte-Puro and Ink4a/Arf$^{-/-}$ astrocyte-Akt-myr cells after treatment with etoposide, whereas an increase of ~2-fold was observed in the nonapoptotic cell population (left upper window that possesses propidium iodide–positive + Annexin V–negative cell population) in the Ink4a/Arf$^{-/-}$ astrocyte-Akt-myr cells compared with Ink4a/Arf$^{-/-}$ astrocyte-Puro cells after treatment with etoposide (Fig. 4C, *top*). Similar to the Ink4a/Arf$^{-/-}$ astrocyte cells, nonapoptotic cell death was significantly elevated in the U87MG-Akt-myr cells compared with the U87MG-Puro cells after treatment with etoposide (Fig. 4C, *bottom*). Taken together, these results indicate that etoposide-specific cell death in the oncogenic Akt-transduced Ink4a/Arf$^{-/-}$ astrocytes and U87MG cells may have resulted from nonapoptotic cell death.

p53-Independent Cell Death of Oncogenic Akt-Transduced U87MG Cells by Etoposide

Because etoposide is known to induce p53-dependent cell death by stimulating DNA damage through the inhibition of topoisomerase II, and Ink4a/Arf$^{-/-}$ astrocytes and U87MG cells possess a normal p53 tumor suppressor

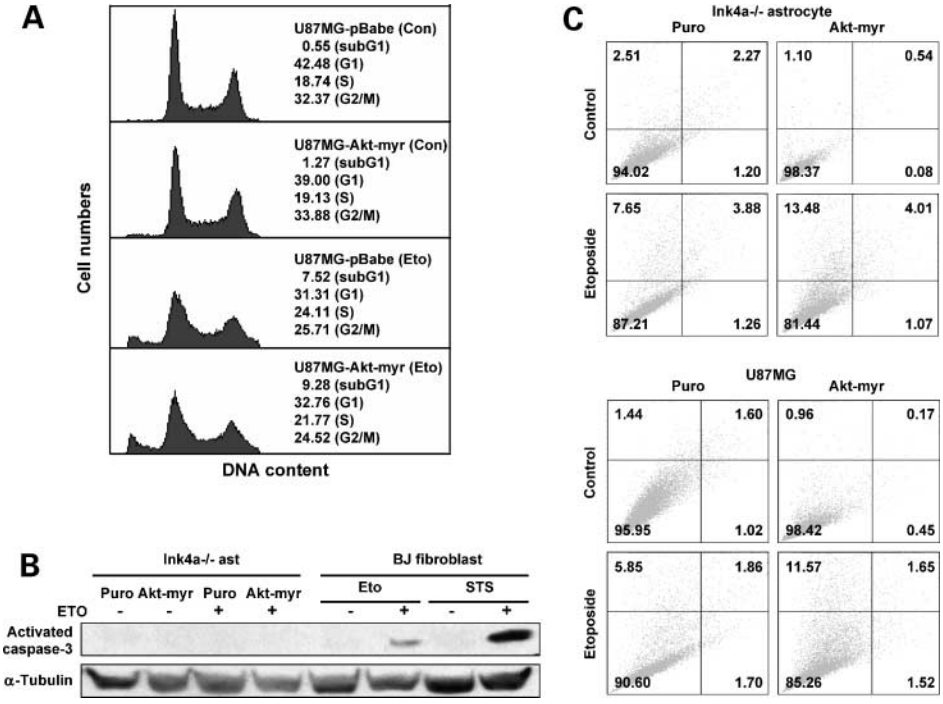

Figure 4. Nonapoptotic cell death of oncogenic Akt-transduced U87MG and Ink4a/Arf$^{-/-}$ astrocyte cells by etoposide. **A,** apoptotic cell death of U87MG-pBabe and U87MG-Akt-myr cells treated without or with etoposide (60 μmol/L for 48 h) was measured by FACS-based quantification of the sub-G_1 cell population. **B,** activated caspase-3 of Ink4a/Arf$^{-/-}$ astrocytes transduced with control vector and Akt-myr treated without or with etoposide (60 μmol/L for 48 h) was determined by Western blot analysis with activated caspase-3–specific antibody. BJ fibroblasts treated without or with etoposide (*Eto*) and staurosporine (*STS*) were used as positive control. **C,** apoptotic cell death (right upper and right lower windows) and nonapoptotic cell death (left upper window) of Ink4a/Arf$^{-/-}$ astrocytes (*top*) and U87MG cells (*bottom*) transduced with control vector and Akt-myr were treated without or with etoposide. Apoptotic cell death (right upper and right lower windows) and nonapoptotic cell death (left upper window) were measured by propidium iodide/Annexin V-FITC staining and FACS-based quantification.

gene (8), we determined whether p53 function is associated with etoposide-mediated selective cell death in the Akt-myr–transduced Ink4a/Arf$^{-/-}$ astrocytes and U87MG cells. Expression of p21^{WAF1} mRNA, one of the p53-downstream transcriptional target genes, was significantly elevated in both U87MG-Puro and U87MG-Akt-myr cells after treatment with etoposide compared with etoposide-untreated cells. However, no significant change was observed in the relative expression level of p21^{WAF1} mRNA between Puro- and Akt-myr–transduced U87MG cells that were treated with etoposide (Fig. 5A). Consistent with the expression levels of p21^{WAF1} mRNA, p21^{WAF1} and BAX proteins were shown to be up-regulated in both U87MG-Puro and U87MG-Akt-myr cells after treatment with etoposide, but no significant difference was observed in the expression levels of the Puro- and Akt-myr–transduced U87MG cells after treatment with etoposide (Fig. 5B). To further test that p53 function is directly associated with selective killing of the Akt-myr–transduced U87MG cells by etoposide, we established p53-inactivated U87MG-Puro and U87MG-Akt-myr cells by transducing *p53DD*, a dominant-negative p53 gene (Fig. 5C). Compared with U87MG-Puro and U87-Akt-myr cells treated with etoposide, we found that the expression of p21^{WAF1} protein was not decreased in the U87MG-Puro + p53DD and U87MG-Akt-myr + p53DD cells treated with etoposide (Fig. 5C). As with U87MG-Akt-myr cells, U87MG-Akt-myr + p53DD cells were shown to be sensitive to etoposide-mediated cell death (Fig. 5D). Taken together, although expression of p21^{WAF1} and BAX genes seems to be elevated in the control and Akt-myr–transduced U87MG cells, p53 tumor suppressor might not be directly associated with the etoposide-dependent selective killing of the Akt-myr–transduced cells.

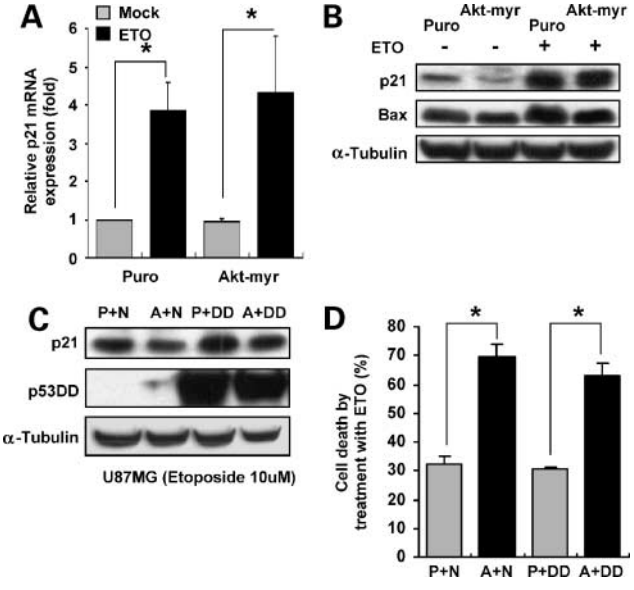

Figure 5. p53-independent cell death of oncogenic Akt-transduced U87MG by etoposide. **A,** expression of p21^{WAF1} mRNA in U87MG-Puro and U87MG-Akt-myr cells treated without or with etoposide (*ETO*; 60 μmol/L) was determined by semiquantitative reverse transcription-PCR. *Columns,* mean (n = 3); *bars,* SE. *, $P < 0.01$, significant difference. **B,** expression of p21^{WAF1} and BAX proteins in the U87MG-Puro and U87MG-Akt-myr cells treated without or with etoposide (60 μmol/L) was measured by Western blot analysis. **C,** U87MG-Puro and U87MG-Akt-myr cells transduced with p53DD (*P* + *N*, Puro + Neo; *A* + *N*, Akt-myr + Neo; *P* + *DD*, Puro + p53DD; *A* + *DD*, Akt-myr + p53DD) were treated with etoposide (10 μmol/L) for 48 h. Expression of p53DD and p21^{WAF1} proteins was determined by Western blot analysis. **D,** cell death rates of p53DD-transduced U87MG-Puro and U87MG-Akt-myr cells (*P* + *N*, Puro + Neo; *A* + *N*, Akt-myr + Neo; *P* + *DD*, Puro + p53DD; *A* + *DD*, Akt-myr + p53DD) grown in the absence or presence of etoposide was determined by the standard trypan blue exclusion method. *Columns,* mean (n = 3); *bars,* SE. *, $P < 0.01$, significant difference.

ROS-Dependent Cell Death of Oncogenic Akt-Transduced U87MG and Ink4a/Arf$^{-/-}$ Astrocyte Cells by Etoposide

Because a previous report has shown that the increased cellular ROS stimulates the expression of p21^{WAF1} in a p53-independent manner (9), we measured cellular ROS levels in U87MG-Puro and U87MG-Akt-myr cells treated without or with etoposide (10 μmol/L) by FACS-based quantification of fluorescent 2′,7′-dichlorofluorescein diacetate (7). As shown in Fig. 6A, cellular ROS levels were moderately elevated in the U87MG-Akt-myr cells compared with U87MG-Puro cells grown in the absence of etoposide, whereas both U87MG-Puro and U87MG-Akt-myr cells displayed marked accumulation of ROS after treatment with etoposide. However, cellular ROS accumulation was clearly higher in the U87MG-Akt-myr cells than in the U87MG-Puro cells grown in the presence of etoposide (Fig. 6A). The elevated ROS did not result from the alteration of antioxidant gene expression in these cells because there was no change in the expressions of manganese superoxide dismutase, copper/zinc superoxide dismutase, catalase, and GPX in the Puro- and Akt-myr–transduced Ink4a/Arf$^{-/-}$ astrocytes and U87MG cells (data not shown).

To further evaluate whether excessive ROS accumulation in the Akt-myr–transduced cells after treatment with etoposide is directly associated with increased cell death, we inhibited cellular ROS accumulation in the etoposide-treated control and Akt-myr–transduced cells by treatment with *N*-acetyl-L-cysteine (a ROS scavenger; Supplementary Fig. S3).[4] The etoposide-mediated cell death in both Puro- and Akt-myr–transduced Ink4a/Arf$^{-/-}$ astrocytes or U87MG cells was dramatically decreased when grown in the presence of *N*-acetyl-L-cysteine (50 mmol/L), showing somewhat similar cell death resistance in these cells (Fig. 6B). These results indicate that etoposide stimulates cellular ROS accumulation and sensitizes the Akt-myr–transduced cells to ROS-mediated cell death. In addition, as treated with different concentration of Paraquat (a ROS generator; Supplementary Fig. S4),[4] both Akt-myr–transduced Ink4a/Arf$^{-/-}$ astrocytes and U87MG cells were more sensitive to cell death than the Puro-transduced counterpart cells (Fig. 6C). Taken together, our observation suggests that treatment of the Akt-myr–transduced cells with etoposide would result in excessive ROS accumulation to a threshold that triggers cell death.

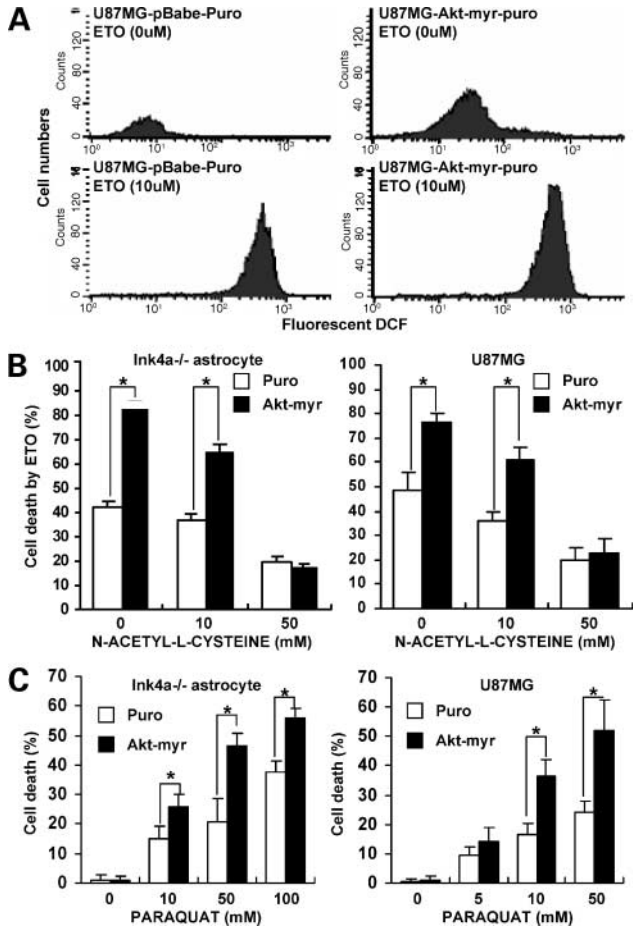

Figure 6. ROS-dependent cell death of oncogenic Akt-transduced U87MG and Ink4a/Arf$^{-/-}$ astrocyte cells by etoposide. **A,** cellular ROS levels in U87MG-Puro and U87MG-Akt-myr cells treated without or with etoposide (10 μmol/L) were measured by FACS-based quantification of fluorescent 2′,7′-dichlorofluorescein diacetate. **B,** Ink4a/Arf$^{-/-}$ astrocytes (*left*) and U87MG cells (*right*) transduced with control vector and Akt-myr were treated without or with etoposide and *N*-acetyl-L-cysteine (a ROS scavenger). Cell death rates were determined by the trypan blue exclusion method. *Columns,* mean (n = 3); *bars,* SE. *, $P < 0.01$, significant difference. **C,** Ink4a/Arf$^{-/-}$ astrocytes (*left*) and U87MG cells (*right*) transduced with control vector and Akt-myr were treated without or with Paraquat (a ROS inducer). Cell death rates were determined by the trypan blue exclusion method. *Columns,* mean (n = 3); *bars,* SE. *, $P < 0.05$, significant difference.

Partial Attenuation of Etoposide-Dependent Cell Death of Oncogenic Akt-Transduced U87MG and Ink4a/Arf$^{-/-}$ by Pepstatin A

Because accumulated evidence has documented that ROS-mediated cell death is associated with lysosomal damage (10), we treated the control and Akt-myr–transduced Ink4a/Arf$^{-/-}$ astrocytes and U87MG cells with pepstatin A (a lysosomal protease inhibitor), which effectively inhibited the ROS and lysosomal damage-mediated cell death (11). The cell death in the Puro- and Akt-myr–transduced Ink4a/Arf$^{-/-}$ astrocytes (Supplementary Fig. S5A)[4] and U87MG cells (Supplementary Fig. S5B)[4] grown in the presence of etoposide was significantly decreased by treatment with pepstatin A (10 μmol/L). However, we found that pepstatin A treatment failed to completely block etoposide-induced death, and expression of lysosomal proteases, such as calpain-1 and calpain-2, which have been implicated in lysosome-mediated cell death (12), was not changed in these cells (data not shown). Therefore, we measured cellular ROS levels in the etoposide-treated Ink4a/Arf$^{-/-}$ astrocyte-Puro and Ink4a/Arf$^{-/-}$ astrocyte-Akt-myr cells by FACS-based quantification of fluorescent 2′,7′-dichlorofluorescein diacetate. Although the cellular ROS accumulation in the etoposide-treated control and Akt-myr–transduced cells was markedly decreased by treatment with pepstatin A, a small population of these cells was found to possess even higher levels of cellular ROS compared with the pepstatin A–untreated counterpart cells (only etoposide-treated cells; Supplementary Fig. S5C),[4] indicating that the failure of complete blockage of cell death by treatment of pepstatin A (Supplementary Fig. S5A and S5B)[4] in the etoposide-treated cells may be due to a small population of cells that possess higher cellular ROS. Taken together, these results suggest that etoposide-mediated cell death in the control and Akt-myr–transduced cells may be in part associated with ROS generation and lysosomal damage.

Discussion

Recently, many research groups have established several human and mouse cancer cells with defined genetic elements to determine the critical genes and pathways that are involved in tumorigenesis (13). The rationales that caused us to use astrocyte cells derived from Ink4a/Arf$^{-/-}$ knockout mice to establish genetically modified cancer cells in the present study are the following: (*a*) the most common brain tumor is the malignant astrocytoma (grades 3 and 4; anaplastic astrocytoma and glioblastoma multiforme), which is derived from astrocyte cells (14) and (*b*) the most common genetic alteration observed in the malignant astrocytoma is the INK4a/ARF loss of function by deletion or epigenetic silence (INK4a/ARF promoter methylation; ref. 15). Primary Ink4a/Arf$^{-/-}$ mouse astrocyte cells used here showed an immortalized phenotype without transformed property (2). As shown by several *in vivo* mouse model studies (16), transduction of activated EGFR, RAS, and Akt, all of which are deregulated in the human malignant astrocytoma by amplification and/or overexpression or alteration in their signaling pathways (1), caused the primary Ink4a/Arf$^{-/-}$ astrocyte cells to become transformed cells. In addition, we used human U87MG glioma cells to create the oncogene-transduced cells because the U87MG cells are known to not have activated EGFR, RAS, and Akt (8), although PTEN tumor suppressor, an inhibitor of phosphatidylinositol 3-kinase/Akt signaling, is inactivated by deletion in these cells (17).

Among numerous known anticancer compounds, we tested four anticancer compounds (staurosporine,

carmustine, doxorubicin, and etoposide), all of which are currently in clinical use, to determine their cytotoxicity to the oncogene-transduced Ink4a/Arf$^{-/-}$ astrocytes and U87MG cells. Interestingly, etoposide, but not doxorubicin, caused selective killing of Akt-myr–transduced cancer cells in a dose- and time-dependent manner because both etoposide and doxorubicin are known to exert their cytotoxicities through the inhibition of a topoisomerase II, which causes DNA damage and concomitant growth arrest or apoptosis by activation of p53 tumor suppressor. In addition, unlike with doxorubicin, etoposide-selective cytotoxicity in the Akt-myr–transduced cells was caused by a p53-independent nonapoptotic cell death. Several recent data have shown that etoposide provokes non-apoptotic cell death via activation of an autophagy-mediated mechanism in the apoptotic signaling–decreased cells, such as proapoptotic Bax/Bak double-knockout fibroblast cells (18, 19). However, the etoposide-selective cytotoxicity in the Akt-myr–transduced cells is not caused by the autophagy-mediated mechanism, as judged by the following: (*a*) no changes in expression of ATG genes (autophagolysosome component genes) and (*b*) the lack of autophagolysosome formation, which is determined using an autophagolysosome marker, GFP-LC3 (ref. 20; data not shown). Therefore, our results suggest that etoposide might possess an uncharacterized cytotoxic function, regardless of the induction of DNA damage by the inhibition of topoisomerase II.

Several studies have documented that when cells possessing inactive apoptotic signaling pathways are exposed to excessive cytotoxic stress, they still display necrotic cell death (21). About this concept, we assume that the apoptotic signaling pathways might be inactivated in the cells used in the present study, in that (*a*) the Ink4a/Arf loss of function per se confers an apoptotic resistance (Ink4a/Arf$^{-/-}$ astrocytes and U87MG control cells; ref. 22) and (*b*) the activated Akt allows cells to be resistant to apoptotic stress by directly inhibiting proapoptotic Bad and the forkhead family of transcription factors (Akt-myr–transduced cells; ref. 23).

Depending on their levels and duration, ROS can cause cellular damage in normal cells, whereas most malignant cancer cells with increased metabolic activity possess an accumulated ROS that plays a crucial role in cell growth and proliferation (24, 25). This indicates that the cell death or cell proliferation triggered by cellular ROS levels should be regulated by a threshold. Similar to our observation in the present study, activation of RAS signaling in the immortalized cells has been shown to stimulate cellular ROS accumulation, which sensitizes oncogenically transformed cells to be killed by β-phenylethyl isothiocyanate, which can induce severe accumulation of cellular ROS by disruption of the glutathione antioxidant system (7). Furthermore, increased ROS has been shown to induce expression of p21^{WAF1} in a p53-independent pathway (9) and results in the development of necrotic cell death through secondary lysosomal damage (11). Therefore, our results indicate that increased ROS accumulation, p53-independent p21^{WAF1} expression, and elevated etoposide-selective cytotoxicity in the Akt-myr–transduced cells should be attributed to activation of Akt, which is one of the cellular components activated by the RAS-phosphatidylinositol 3-kinase signaling pathway.

In conclusion, we used genetically modified cancer cells to show that etoposide exerts a novel therapeutic activity that allows the oncogenic Akt-transduced cancer cells to kill preferentially through ROS-mediated damage. Therefore, these genetically modified cancer cells should permit us to identify oncogene-targeted agents and those for its related pathway from either known or novel compounds, which may allow for the development of ideal anticancer drugs, which would be toxic to cancer cells with minimum toxicity to normal cells.

Acknowledgments

We thank Dr. Tamotsu Yoshimori (Osaka University, Osaka, Japan) for providing GFP-LC3 vector and Ho-Yeon Oh for statistical analysis.

References

1. Maher EA, Furnari FB, Bachoo RM, et al. Malignant glioma: genetics and biology of a grave matter. Genes Dev 2001;15:1311 – 33.

2. Bachoo RM, Maher EA, Ligon KL, et al. Epidermal growth factor receptor and Ink4a/Arf: convergent mechanisms governing terminal differentiation and transformation along the neural stem cell to astrocyte axis. Cancer Cell 2002;1:269 – 77.

3. Capdeville R, Buchdunger E, Zimmermann J, Matter A. Glivec (STI571, imatinib), a rationally developed, targeted anticancer drug. Nat Rev Drug Discov 2002;1:493 – 502.

4. Mokbel K, Hassanally D. From HER2 to Herceptin. Curr Med Res Opin 2001;17:51 – 9.

5. Shawver LK, Slamon D, Ullrich A. Smart drugs: tyrosine kinase inhibitors in cancer therapy. Cancer Cell 2002;1:117 – 23.

6. McCarthy KD, de Vellis J. Preparation of separate astroglial and oligodendroglial cell cultures from rat cerebral tissue. J Cell Biol 1980;85: 890 – 902.

7. Trachootham D, Zhou Y, Zhang H, et al. Selective killing of oncogenically transformed cells through a ROS-mediated mechanism by β-phenylethyl isothiocyanate. Cancer Cell 2006;10:241 – 52.

8. Ishii N, Maier D, Merlo A, et al. Frequent co-alterations of TP53, p16/CDKN2A, p14ARF, PTEN tumor suppressor genes in human glioma cell lines. Brain Pathol 1999;9:469 – 79.

9. Russo T, Zambrano N, Esposito F, et al. A p53-independent pathway for activation of WAF1/CIP1 expression following oxidative stress. J Biol Chem 1995;270:29386 – 91.

10. Nohl H, Gille L. Lysosomal ROS formation. Redox Rep 2005;10: 199 – 205.

11. Raymond MA, Mollica L, Vigneault N, et al. Blockade of the apoptotic machinery by cyclosporin A redirects cell death toward necrosis in arterial endothelial cells: regulation by reactive oxygen species and cathepsin D. FASEB J 2003;17:515 – 7.

12. Demarchi F, Schneider C. The calpain system as a modulator of stress/damage response. Cell Cycle 2007;6:136 – 8.

13. Hahn WC, Weinberg RA. Modeling the molecular circuitry of cancer. Nat Rev Cancer 2002;2:331 – 41.

14. Behin A, Hoang-Xuan K, Carpentier AF, Delattre JY. Primary brain tumors in adults. Lancet 2003;361:323 – 31.

15. Nishikawa R, Furnari FB, Lin H, et al. Loss of P16INK4 expression is frequent in high grade gliomas. Cancer Res 1995;55:1941 – 5.

16. Holland EC. Gliomagenesis: genetic alterations and mouse models. Nat Rev Genet 2001;2:120 – 9.

17. Maehama T, Dixon JE. PTEN: a tumour suppressor that functions as a phospholipids phosphatase. Trends Cell Biol 1999;9:125 – 8.

18. Shimizu S, Kanaseki T, Mizushima N, et al. Role of Bcl-2 family proteins in a non-apoptotic programmed cell death dependent on autophagy genes. Nat Cell Biol 2004;6:1221 – 8.

19. Kim R, Emi M, Tanabe K. Caspase-dependent and -independent cell death pathways after DNA damage. Oncol Rep 2005;14:595 – 9.

20. Crighton D, Wilkinson S, O'Prey J, et al. DRAM, a p53-induced modulator of autophagy, is critical for apoptosis. Cell 2006;126:121 – 34.

21. Nicotera P, Melino G. Regulation of the apoptosis-necrosis switch. Oncogene 2004;23:2757 – 65.

22. Serrano M, Lee H, Chin L, Cordon-Cardo C, Beach D, DePinho RA. Role of the INK4a locus in tumor suppression and cell mortality. Cell 1996; 85:27 – 37.

23. Downward J. PI3-kinase, Akt, and cell survival. Semin Cell Dev Biol 2004;15:177 – 82.

24. Irani K, Xia Y, Zweier JL, et al. Mitogenic signaling mediated by oxidants in Ras-transformed fibroblasts. Science 1997;275:1649 – 52.

25. Chen QM, Bartholomew JC, Campisi J, Acosta M, Reagan JD, Ames BN. Molecular analysis of H_2O_2-induced senescent-like growth arrest in normal human fibroblasts: p53 and Rb control G_1 arrest but not cell replication. Biochem 1998;332:43 – 50.